Progress in the theoretical description and experimental characterisation of impurity transport in ASDEX Upgrade

F.J. Casson, C. Angioni, R. Dux, B. Geiger, R.M. McDermott, L. Menchero[(1)]
A.G. Peeters[2], C. Veth, and ASDEX Upgrade team
Max-Planck-Institut für Plasmaphysik, Garching bei München, Germany
[1] *University of Strathclyde, United Kingdom;* [2] *University of Bayreuth, Germany*

The core charge exchange (CX) diagnostic on ASDEX Upgrade (AUG) was substantially upgraded prior to the 2011 campaign to a 30 channel system which provides much higher temporal resolution and more complete profiles as compared with the previous system [1]. This system is routinely used to provide high resolution measurements of ion temperature and rotation. Impurity densities can also be calculated from the CX spectra, but this analysis is more challenging, because it requires correct treatment of the neutral beam attenuation and halo contributions up to at least the second excited state [2]. The impurity concentration analysis CHICA code, used for these calculations, has recently been substantially rewritten to model these contributions more accurately, and now includes an improved beam geometry based on beam emission spectroscopy measurements, more accurate modelling of the beam excited state populations, a calculation of the halo population through the FIDASIM code [3], and inclusion of the halo contribution to the CX signal using ADAS thermal charge exchange cross-sections [4]. The overall result of these improvements has been to reduce the calculated boron densities to $\sim$ 40% of their value in the previous simpler analysis (the logarithmic gradients, by contrast, are relatively unchanged).

For this work, a database of boron density profiles from H-mode shots from the 2011 campaign has been constructed. The database is created from 29 steady phases of at least 0.5 seconds from 10 shots. All shots have a continuous 2.5 MW NBI heating power from the beam used for the CX measurements. This heating provides a minimum to which additional NBI and ECRH heating are added (shots with ICRH are excluded). The database covers a range of plasmas with plasma currents I_p from 0.6 to 1.0 MA, NBI powers between 2.5 and 7.5 MW, ECRH powers from 0 to 2.5 MW, core electron densities between 5 and 9 $\cdot 10^{-19} m^{-3}$, Greenwald fraction n_e/n_{GW} = 0.35-0.85, β_N = 0.65-2.0, and safety factor q_{95} = 3.9-7.1. All plasmas are lower single null with toroidal field -2.5T and similar edge elongation (1.6) and triangularity (0.15).

A number of strong correlations are visible in the database (Fig. 1). The most striking is between the Mach number $u = v_{tor}/v_{th_i}$ and the logarithmic gradient of the boron density, R/L_{nB}. Similar correlations can also be seen between R/L_{nB} and both $u' = -(R/v_{th_i})du/dr$ and NBI power, since both of these quantities are trivially correlated with the Mach number. The relationship between rotation and impurity peaking is the result of a rather complex chain of causality: When moderate electron heating is applied to an NBI heated (ITG dominated) H-mode in AUG, there is a rather generic observation of increased density peaking and decreased rotation (the opposite is true if electron heating is applied to a TEM dominated plasma) [5]. The density peaking occurs when the dominant modes are shifted from strong ITG towards the TEM transition, since

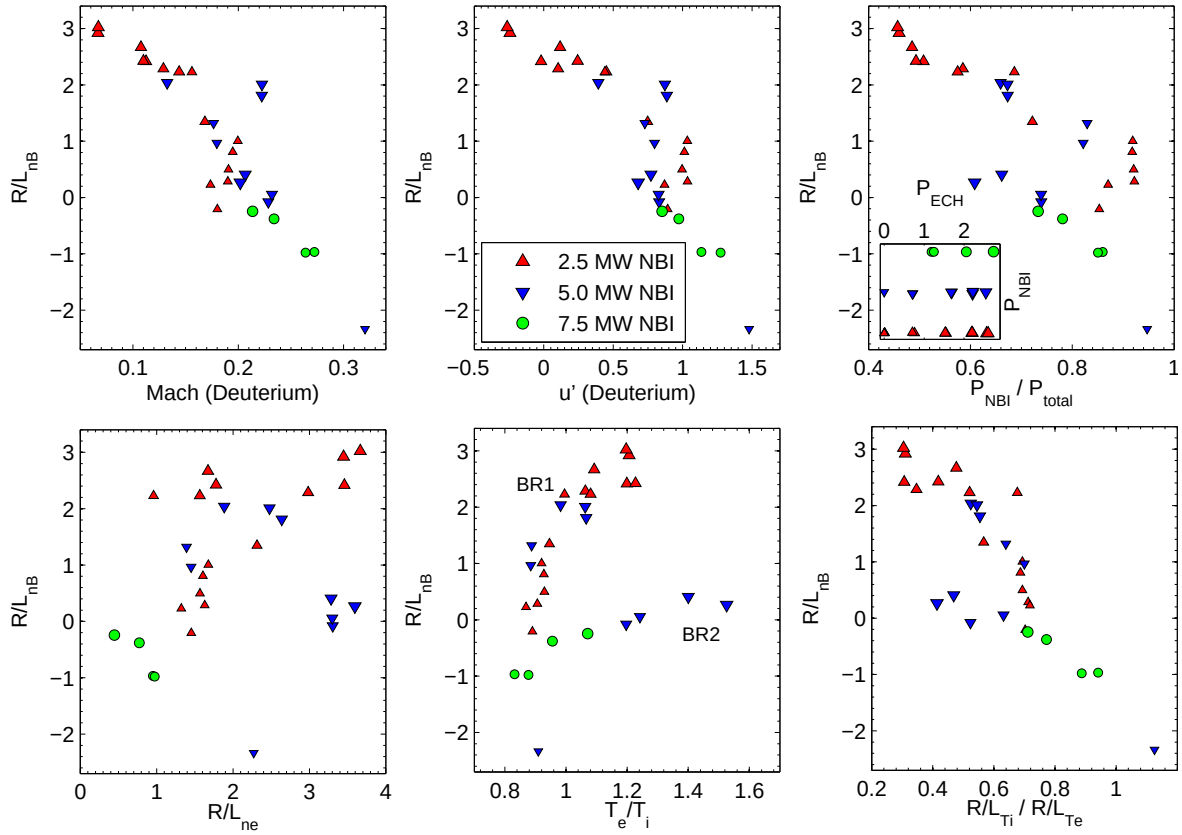

Figure 1: Correlations in the AUG experimental H-mode dataset of boron density measurements at $r/a = 0.5$. The size of the points indicates the ECRH heating power between 0 and 2.5 MW, the colour of the points represents the NBI heating power between 2.5 and 7.5 MW.

the transition is the region with the strongest convective particle pinch [7, 8]. The decreased rotation then follows as a consequence, possibly due to an inward residual stress which increases with the density gradient [9]. Since NBI heating drives rotation and ITG turbulence, while ECRH heating reduces rotation and moves the dominant mode toward TEM, a correlation between the mode frequency and plasma rotation is found for each mode.

The impurity flux can be decomposed as

$$\Gamma_s = n_s D_s \left(\frac{R}{L_n}\bigg|_{R_{LFS}} + C_T \frac{R}{L_T} + C_u u' + C_p \right) \tag{1}$$

where the individual terms correspond to the diffusive, thermo-diffusive, roto-diffusive, and convective parts, respectively. The roto-diffusive term is a result of symmetry breaking mechanisms and is therefore closely connected with the mechanisms of momentum transport [6, 8].

The boron density gradients are correlated with the electron density gradients because the same convective pinch mechanism applies to all species. For impurities, the roto- and thermo-diffusive terms reduce the boron density peaking relative to the electron density peaking (for electrons, roto-diffusion is neglible, and thermo-diffusion has opposite sign). The contributions from both terms increases with the ITG character of the mode (correlated with the NBI heating and rota-

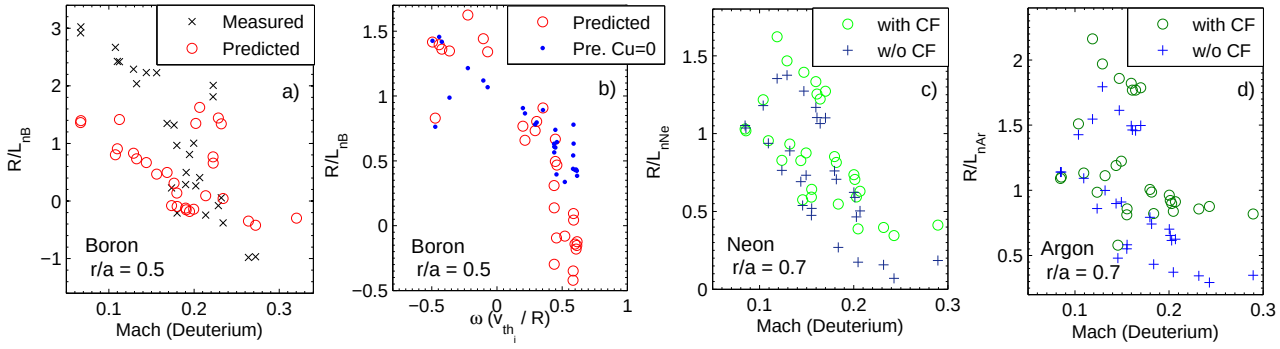

Figure 2: a) Predicted and measured values of R/L_{nB} at $r/a = 0.5$. b) Comparison of the boron predictions including and excluding the contribution from roto-diffusion. The frequency is determined from the frequency of the mode at $k_\theta \rho_s = 0.3$, with negative values indicating TEM and positive ITG. c,d) Predicted values of R/L_{nZ} (low field side) for neon and argon at $r/a = 0.7$ for the same shot database as boron, with and without centrifugal effects.

tion), and the roto-diffusive contribution is also directly proportional to the rotation gradient.

To summarise, in ITG dominated H-modes, electron heating causes density peaking (by moving the turbulence towards the TEM transition), density peaking causes rotation flattening, which allows increased impurity peaking because the roto-diffusive term is reduced. We have seen some evidence of this chain of causality in the transient response of the profiles after the switch on of ECRH; this awaits a more systematic analysis. In addition, the mode frequency, which also influences the impurity response is correlated with the rotation due to the momentum imparted by NBI heating and the rotation flattening with ECRH heating.

To verify our understanding of these complex interdependencies, quasilinear simulations were conducted for each point in the dataset with the gyrokinetic code GKW [10],with a spectrum [12] with a peak at $k_\theta \rho_s = 0.3$. The impurities are modelled in the trace limit such that the drift-wave is completely determined by the bulk plasma conditions. Neoclassical transport is neglible for these cases [11] and is not included. Electromagnetic fluctuations are neglected and are expected to give only minor flattening for these cases [13] (which mostly have $\beta < 0.5\%$). The impurity transport dimensionless coefficients C_T, C_u, and C_p are then a linear response to the impurity gradients, and are calculated from 4 trace species with an orthogonal set of gradients. The steady state impurity density gradient is then predicted independently of any impurity measurement and compared with the experimental data (Fig. 2).

The correlation between R/L_{nB} and Mach number is well captured by the modelling, which gives confidence that most of the underlying mechanisms are correctly described. Some of the modelling outliers to the trend may be improved by examining the sensitivity to input parameters. The q profile, which is the most uncertain of the inputs, can have a strong impact on the TEM cases, such as the 4 outliers in the predicted values at high Mach and high R/L_{nB}.

However, it is clear that the modelling consistently underpredicts both the peaking and hollowness of the boron density profiles by a factor of about 2; a fact which was evident in Ref. [11], but is here clarified by the extended parameter regime. It is difficult to argue that uncertainties

in the inputs to the simulations can cause such a systematic effect, and one must conclude that either the methodology of the modelling or the density measurement is missing an important feature. On the modelling side, the use of a more realistic spectrum could increase the predicted R/L_{nB} for the TEM cases. For the higher Mach number ITG cases, additional symmetry breaking effects not included in these simulations (such as those invoked for the residual stress [9]) might increase the roto-diffusive term, giving more hollow predicted gradients (we plan to investigate both with nonlinear simulations).

The GKW code includes the centrifugal force [14] and has recently been updated with the rotation gradient in the centrifugal effects to allow prediction of 2D density distributions (Fig. 3). The effects are dramatic for heavy impurities such as tungsten. Centrifugal effects are included in the boron predictions, but have only a minor impact. Argon and neon impurities were also modelled for the same database to estimate the magnitude of the centrifugal effects for heavier impurities which may in the future be measured with charge exchange (which would allow easy direct comparison with a *localised* LFS measurement). Generally, the centrifugal effects decrease the predicted $R/L_{nZ}|_{LFS}$ for $r/a < 0.5$ and increase it for $r/a > 0.5$, which is a consequence of the outward shift of the impurity relative to the flux surfaces. At $r/a = 0.5$, competing centrifugal effects cancel out such that the prediction of $R/L_{nZ}|_{LFS}$ is not usually significantly changed. At higher Mach numbers, the centrifugal effects can change the predicted $R/L_{nZ}|_{LFS}$ of argon at $r/a = 0.7$ by up to 0.8, which should be measurable (Fig. 2).

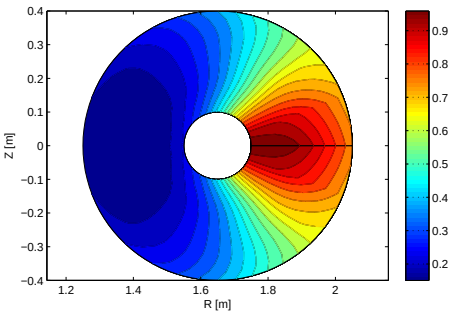

Figure 3: GKW prediction of the poloidal cross section of the density of W 46+ for a NBI heated AUG H-mode, with core deuterium Mach no. $u = 0.22$ (Tungsten u_W = 2.1). Maximum density is normalised to 1. Flux surfaces are concentric circles.

References

[1] R. M. McDermott et al. Plasma Phys. Control. Fusion, **53**, 124013 (2011)

[2] R. Dux. et al., EPS Plasma Phys. Conference, Poster P2.049 (2012)

[3] B. Geiger et al., Plasma Phys. Control. Fusion, **53**, 065010 (2011)

[4] R Hoekstra, et al., Plasma Phys. Control. Fusion **40**, 1541 (1998);
H. P. Summers, ADAS User Manual 2.6, http://www.adas.ac.uk, (2004).

[5] R.M. McDermott et al. Plasma Phys. Control. Fusion, **53**, 035007 (2011)

[6] Y.Camenen et al., Phys. Plasmas, **16**, 012503, (2009)

[7] E. Fable et al., Plasma Phys. Control. Fusion **52**, 015007 (2010)

[8] C. Angioni et al., *Off-diagonal particle and toroidal momentum transport: A survey of experimental, theoretical, and modelling aspects, In press*, Nucl. Fusion (2012)

[9] C. Angioni et al., Phys. Rev. Lett. **107**, 215003 (2011)

[10] A.G. Peeters et al., Comp. Phys. Commun., **180**, 2650 (2009)

[11] C. Angioni et al., Nucl. Fusion **51**, 023006 (2011)

[12] A. Casati et al., Nucl. Fusion **49**, 085012 (2009)

[13] T. Hein and C. Angioni, Phys. Plasmas. **17**, 012307 (2010)

[14] F. J. Casson et al., Phys. Plasmas **17**, 102305 (2010)